COMMUNICATIONS

Magnetic Resonance in Medicine 48:927–933 (2002)

Dynamic Activity-Induced Manganese-Dependent Contrast Magnetic Resonance Imaging (DAIM MRI)

Ichio Aoki,[1,4*] Chuzo Tanaka,[1] Tetsuro Takegami,[2] Toshihiko Ebisu,[1] Masahiro Umeda,[1] Masaki Fukunaga,[1] Kohji Fukuda,[3] Afonso C. Silva,[4] Alan P. Koretsky,[4] and Shoji Naruse[5]

Activity-induced manganese-dependent contrast (AIM) MRI is a hemodynamic-independent functional MRI method that used manganese ion as an MR-detectable contrast agent. In AIM, $MnCl_2$ is infused intra-arterially after the blood-brain barrier (BBB) is opened with a hyperosmolar agent. Upon functional stimulation of the brain, Mn^{2+} accumulates in the active region(s) by entering active cells through voltage-gated Ca^{2+} channels, causing local signal increases in T_1-weighted images. The contrast of AIM MRI depends strongly on the depth of anesthesia, and the low levels used in somatosensory stimulation studies can lead to significant nonspecific accumulation of manganese ion throughout the brain. The purpose of this study was to produce an AIM functional map of somatosensory stimulation, which separates the stimulation-specific signal increase from the nonspecific activation due to light anesthesia. A dynamic AIM (DAIM) paradigm was developed, which used sequential MR scans during $MnCl_2$ infusion, prior to and following functional stimulation of the brain. Stimulation-specific functional maps were produced using time-course analysis. The new method was tested during glutamate administration and electric stimulation of the rat forepaw. It was shown that DAIM maps are better confined to the specific region of brain activated by somatosensory stimulation as compared to AIM MRI. Magn Reson Med 48:927–933, 2002. © 2002 Wiley-Liss, Inc.

Key words: functional MRI; manganese; brain activity; somatosensory stimulation; calcium channels

Functional MRI (fMRI) techniques based on blood oxygen level-dependent (BOLD) contrast (1) or regional brain perfusion (2) rely on changes of brain hemodynamics during increased neural activity. Recently, a new method for fMRI, termed activity-induced manganese-dependent (AIM) MRI, was described as being independent of hemodynamic changes (3). This method uses manganese ion (Mn^{2+}) as an MR-detectable contrast agent. Mn^{2+} is handled in a manner similar to calcium ion (Ca^{2+}) in many biological systems (4,5), and is known to enter cells through ligand- or voltage-gated Ca^{2+} channels during nerve action potentials (6–9). In addition, Mn^{2+} shortens both the T_1 and T_2 relaxation times of water protons (10–13). In AIM MRI, the Mn^{2+} influx and intracellular accumulation caused by neuronal depolarization shortens the water relaxation times of the activated brain regions and produces enhanced contrast on T_1-weighted MRI. A recent comparison of AIM with BOLD and CBF fMRI of the rat forepaw showed that the activated brain region mapped from the decrease in T_1 is in excellent agreement with that determined from hemodynamic changes (14). AIM MRI can map brain activation with high signal-to-noise (SNR) and contrast-to-noise (CNR) ratios, and at high spatial resolution (3).

AIM MRI has been successfully used to map the forelimb area of the somatosensory cortex in rats anesthetized with alpha-chloralose (14) or a mixture of alpha-chloralose and urethane (3,15–17). However, the functional contrast in AIM MRI has a strong dependence on the depth of anesthesia (15–17). The baseline signal can increase, even in the absence of any stimulation, in awake (3) or lightly anesthetized (15) rats. It has been speculated that such signal elevation comes from accumulation of Mn^{2+} in brain regions that either have an elevated basal (resting) neuronal activity, or are responding to nonspecific or unintended stimuli coming from the surrounding environment, such as sounds, light, or restraint of the animal (15,17). In addition, there are regions of the brain, such as the ventricles, which show enhancement to manganese independent of any stimulation (3,15,16). It is difficult, therefore, to ascertain whether AIM MRI maps are contaminated with baseline signals from any unintended stimulation from the environment.

On the other hand, deep anesthesia levels can inhibit brain activation below detectability. Although encephalographic studies have shown the maintenance of overall brain activity even under deep anesthesia (18), we were unable to detect activation in preliminary AIM experiments during somatosensory stimulation in rat using 2.5% halothane anesthesia (data not shown). Therefore, the optimum anesthetic level is the one that suppresses overall baseline activation without inhibiting activation of intentionally stimulated areas (15).

[1]Department of Neurosurgery, Meiji University of Oriental Medicine, Kyoto, Japan.

[2]Department of Neurosurgery, Kyoto Prefectural University of Medicine, Kyoto, Japan.

[3]Department of Physiology, Meiji University of Oriental Medicine, Kyoto, Japan.

[4]Laboratory of Functional and Molecular Imaging, National Institute of Neurological Disorders and Stroke, Bethesda, Maryland.

[5]Department of Radiology, Kyoto Prefectural University of Medicine, Kyoto, Japan.

Grant sponsors: Special Coordination Funds for Promoting Science and Technology Ministry of Education, Culture, Sports, Science and Technology (MEXT) of Japan; Japanese Society for the Promotion of Science; Grant numbers: 97L00204; 14770726.

*Correspondence to: Ichio Aoki, Ph.D., Department of Medical Informatics, Medical MR Center, Meiji University of Oriental Medicine, Hiyoshi-cho, Funai-gun, Kyoto 629-0392, Japan. E-mail: aoki@muom.meiji-u.ac.jp

Received 23 April 2002; revised 16 August 2002; accepted 21 August 2002.

DOI 10.1002/mrm.10320

Published online in Wiley InterScience (www.interscience.wiley.com).

AIM also shows potential for use in awake, behaving animals (3), in which separating activities caused by specific stimuli can be very challenging. Therefore, it is important to develop approaches that can separate manganese enhancement due to specific stimulation from nonspecific effects. The purpose of this study was to produce brain functional maps using Mn^{2+} as a contrast agent in a way that separates the intended, stimulation-specific signal increases from unintended, nonspecific signals. The brain activation maps that correct for baseline signal increases are calculated using a dynamic measurement paradigm. We call this new approach dynamic AIM (DAIM) MRI. We show that the DAIM maps can reliably differentiate stimulation specific regions from nonspecific "false activation," in comparison with AIM MRI in the same animals.

METHODS

DAIM Paradigm

The original AIM paradigm has been previously described in detail (3). Briefly, a series of T_1-weighted images were acquired after disrupting the blood-brain barrier (BBB) with a hyperosmolar agent, such as D-mannitol, and during a continuous intra-arterial infusion of $MnCl_2$. Stimulation caused Mn^{2+} to accumulate in activated regions of the brain, thus generating functional contrast.

The present study introduces a new approach to produce functional brain maps that accurately reflect the variation of stimulation-specific signals. In this paradigm, four sets of MR images were acquired sequentially under four different conditions. First, in order to observe the variation of signal intensity under the condition in which the BBB is still intact, images were obtained after initiation of the $MnCl_2$ infusion, but before breaking the BBB with a hyperosmolar bolus injection of D-mannitol. This first set of images was obtained to estimate the influence of Mn^{2+} in the vasculature as a relaxing agent for water. In addition, the average of this set was used to normalize relative signal intensities for all subsequent MR images. Next, a bolus injection of D-mannitol was given to open the BBB, and a second set of images was acquired while continuing the $MnCl_2$ infusion, but before functional stimulation. This second set was obtained to estimate the Mn^{2+} accumulation into brain areas caused by nonspecific effects, including basal (resting) neuronal activity; unintended stimuli from the environment, such as acoustical noise, ambient light, and odors; neuronal disinhibition under low-level anesthesia; and possible variation in signal intensity due to the disruption of the BBB by D-mannitol. Subsequently, a third set of images was acquired during functional stimulation, while $MnCl_2$ was still continuously infused. This set was obtained to estimate the Mn^{2+} accumulation in neurons caused by intentional stimulation. The fourth and final set of images was acquired after both the $MnCl_2$ infusion and the functional stimulation were stopped. This fourth set was obtained to estimate the signal reduction caused by decreased Mn^{2+} concentration in blood, and by washout from neurons. In addition, the first few images in this final set were averaged to produce an AIM MRI image.

Animal Preparation

Male Wistar rats (290–330 g; Shimizu Experimental Animals, Japan) were divided into three groups: normal control ($N = 5$), glutamate administration ($N = 5$), and electric forepaw stimulation ($N = 5$). Rats were initially anesthetized with diethyl ether (Nacalai Tesque, Inc., Japan); they were then orally intubated and ventilated with 2.0–2.3% halothane and a 1:1 O_2/room air gas mixture using a rodent ventilator (model 683; Harvard Instruments, MA). Polyethylene catheters (PE-50; Becton Dickinson, MD) were placed in the femoral artery and vein to monitor blood pressure, sample blood gases, and inject drugs. The right external carotid artery was also cannulated for drug administration (19). Arterial blood gases/pH were examined every 30 min in the femoral artery using blood gas/pH analyzer (model 178; Corning, NY). Rectal temperature was maintained at approximately 37°C using warm air during preparation and scanning.

Administration of Agents

Following surgery, a mixture of alpha-chloralose (25 mg/kg; Nacalai Tesque, Inc., Japan) and urethane (450 mg/kg; Aldrich Chemical Company, Inc., Milwaukee, WI) was injected intraperitoneally. Halothane was switched off 15 min after the alpha-chloralose injection. Pancuronium bromide (2.5 mg/kg; Organon, Inc., West Orange, NJ) was injected via the femoral vein for suppression of motion. The rats were then secured inside the MR scanner, and drug administration and image acquisition were performed according to the DAIM paradigm described above. Manganese chloride ($MnCl_2$-$4H_2O$; Sigma, MO), dissolved to 74.5 mM in isotonic saline, was infused via the right carotid artery at a rate of 3.97 μmol/min (3.2 ml/hr) using a syringe pump (model 100; Neuroscience, Inc., Japan) for 32 min. This infusion was started at the same time as the MRI acquisition and was stopped before acquisition of the fourth set of images. The total volume of the infused $MnCl_2$ solution was 1.71 ml (127 μmol). To break the BBB, 25% D-mannitol solution (5 ml/kg) was bolus-injected via the right carotid artery after acquisition of the first set of images (10.6 min after start of the $MnCl_2$ infusion).

Glutamate Administration and Electrical Forepaw Stimulation

In the glutamate administration group, L-glutamic acid solution (0.2 ml of 10 mg/ml; Sigma) was administered through the right carotid artery following the acquisition of the second set of images. In the control group, saline solution (0.2 ml) was injected through the right carotid artery.

For electrical stimulation of the rat forepaw, two needles were inserted under the skin of the left forepaw and were connected to an electric stimulator (Sanei, Inc., Japan). Serial rectangular pulses of 10 V amplitude, 0.2 ms duration, and 2 Hz frequency were used. Stimulation was applied during acquisition of the third set of images.

MRI Measurements

MRI experiments were performed in a 4.7 T horizontal spectrometer (CSI-II-Omega; Bruker, Germany) with a

shielded gradient coil (65 mm diameter). An in-house-made transmit/receive surface coil (25 mm diameter) was used. T_1-weighted, gradient-echo coronal images were obtained using the following parameters: TR = 150 ms, TE = 5.4 ms, matrix size = 64 × 64, flip angle = 50°, FOV = 25 mm, slice thickness = 1 mm, number of averages = 4, number of slices = 4, and interslice gap = 1 mm. The total acquisition time of each T_1-weighted image was 40 s. Sixteen images were acquired for each of the four sets in the DAIM paradigm, resulting in a total of 64 images obtained in 42.7 min (10.7 min per set). Control of the sequential imaging was performed using a C-shell script, which guided the administration of drugs as well as the electrical stimulation.

Data Analysis

Image analysis was performed using Interactive Data Language (IDL; Research Systems, Inc., CO), MRVision (MRVision Co., MA), Adobe Photoshop (Adobe Systems, Inc., Mountain View, CA), and NIH Image (NIH, MD). Data are presented as mean ± standard deviation (SD). Statistical significance was set to $P < 0.01$. Analysis of variance (ANOVA) was used for discrimination of signal changes, and unpaired *t*-tests were applied for comparison of signal intensities from different brain regions.

DAIM Value and DAIM Map Calculations

Regions of interest (ROIs) were set to the entire brain area covered in the coronal images. Relative signal intensities were calculated for all images using the mean of the first set of images as a reference baseline. The logarithm of relative signal intensities was fitted on a pixel-by-pixel basis to a linear function, and slopes were calculated for the second and third image sets. The value of the slope from the third image set was subtracted from the value of the slope from the second image set, yielding the DAIM value:

$$\text{DAIM Value} = -(S_3 - S_2)$$

where S_2 and S_3 are the slopes of the logarithmic regression of the second and third sets of images, respectively. DAIM functional maps were created from the calculated DAIM values for each pixel, except for the ones that did not show good correlation ($r^2 < 0.3$) on the logarithmic regression. These pixels were excluded from the DAIM maps. DAIM maps are displayed using a color scale defined as mean DAIM value ± 2 SD. The image analysis for calculating DAIM values and making DAIM maps was performed using an in-house-made autocalculation procedure on IDL.

RESULTS

The mean arterial blood pressures before and after $MnCl_2$ administration were 111.6 ± 8.1 mmHg and 102.7 ± 12.1 mmHg, respectively. After mannitol injection, the blood pressure dropped by ~12–20 mmHg, but returned to baseline immediately. During stimulation, the mean blood pressure increased by ~10 mmHg and returned to baseline after stimulation. Blood gases and pH were within normal physiological ranges: pH = 7.38 ± 0.15, P_aCO_2 = 38.9 ± 4.2 mmHg, and P_aO_2 = 121.2 ± 8.3 mmHg.

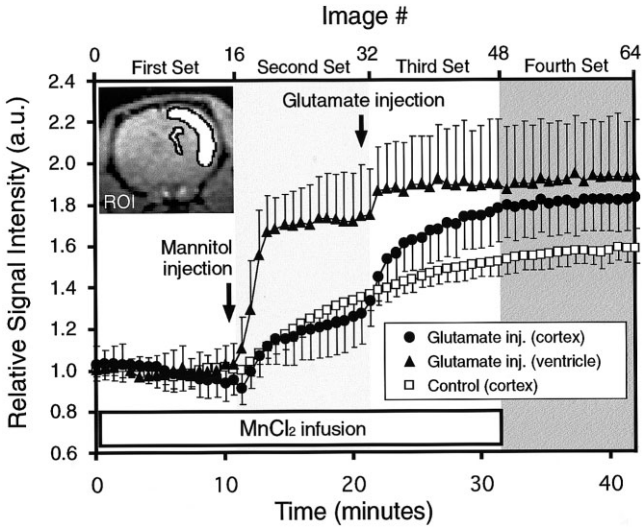

FIG. 1. Typical DAIM time-courses of relative signal intensities in the cortex and ventricle obtained from the glutamate administration (filled symbols) and control (open squares) groups. The inset indicates typical ROIs. The first set of images (#1–16) was obtained before D-mannitol administration, after start of $MnCl_2$ infusion. The second set (#17–32) was obtained before injection of glutamate, after breaking the BBB with mannitol. The signal increases significantly in a nonspecific manner following opening of the BBB. The third set (#33–48) was obtained after glutamate injection. The signal intensity in the cortex of the glutamate administration group (filled circles) increases substantially after glutamate injection, but not in the control group following saline administration (open squares). The fourth set (#49–64) was obtained during rest after stopping the $MnCl_2$ infusion.

Four sets of 16 MR images were acquired according to the DAIM protocol for each of the three groups used in this study: control, glutamate administration, and electrical stimulation. Figure 1 shows typical changes in relative signal intensity for glutamate administration and control from ROIs in the cortex and ventricle. The first set of images (#1–16), obtained after the start of the $MnCl_2$ infusion but before the D-mannitol injection, did not show any significant signal changes. The second set of images (#17–32), acquired after D-mannitol administration for opening the BBB, showed a significant increase of signal intensity in both the cortex and ventricle ($P < 0.01$). A much larger signal increase was observed in the ventricle as compared to the cortex. The third set of images (#33–48), obtained after injection of glutamate, showed a robust signal increase in the cortex ($P < 0.01$). In contrast, the signal increase in the ventricle was not significant ($P > 0.05$). In the control group, a moderate signal increase was observed in the third set of images as compared to the second set. The fourth set of images (#49–64), in which the $MnCl_2$ infusion was stopped, did not show significant changes in signal intensity ($P > 0.05$) in any group.

Figure 2 shows a linear regression plot of signal changes from the second and third sets of images on a semi-logarithmic chart. The data was obtained from the ROIs indi-

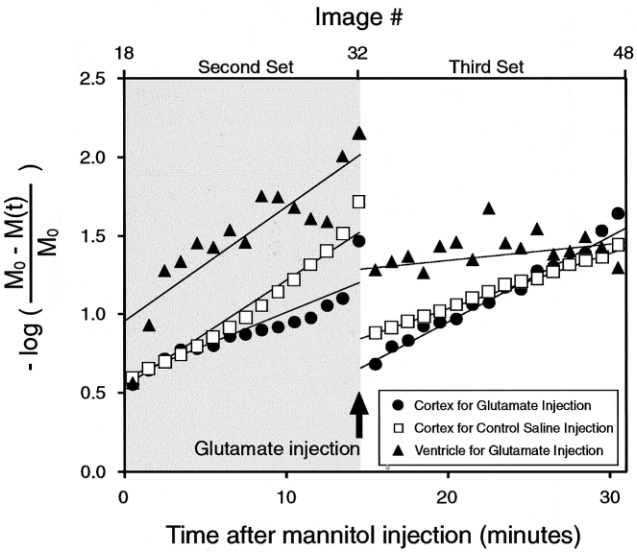

FIG. 2. Logarithmic regression of the time-courses shown in Fig. 1, plotted during the second and third sets of images. In the cortex of the glutamate administration group (filled circles), the slope of the regression line increases significantly after glutamate injection. On the other hand, the slope of the regression line decreases in both the ventricle of the glutamate administration group (filled triangles) and the cortex of the control group (open squares) after injection of glutamate or saline, respectively.

cated in Fig. 1. In the cortex for the glutamate administration group, the slope of the regression line increased somewhat (0.044–0.056) following glutamate administration, as a result of the higher rate of accumulation of Mn^{2+}. On the other hand, in the ventricle ROI from the same group, the slope of regression line decreased substantially (0.077–0.006) because the relative increase in signal intensity after glutamate administration was small. Likewise, in the cortex of the control group, the slope of the regression line decreased significantly following glutamate administration (0.074–0.036), meaning the increase of signal intensity after saline administration was small. In the glutamate administration group, the slopes of the logarithmic regression were increased in the cortex, where stimulation-specific signal changes were expected. In contrast, the slopes were decreased in the ventricle, where stimulation-specific signal changes were not expected. Therefore, the variation of the slopes obtained before and after stimulation can be used to separate stimulation-specific signal changes from nonspecific signal increases.

Figure 3 shows a comparison between DAIM and AIM MRI. The left column shows a typical DAIM functional map (Fig. 3a) and AIM images (Fig. 3b) from the glutamate administration group. High DAIM values were observed in the entire brain hemisphere, except for the ventricles (arrows), which were clearly enhanced in the AIM experiment. In addition, AIM activation was observed in the lower parts of the right hemisphere, but not in the DAIM map. However, because of the lower SNR at the base of the brain caused by the use of a surface coil, many pixels located in this ventral region were excluded from the DAIM map for not passing the $r^2 < 0.3$ threshold imposed in the linear regression analysis. The right column of Fig. 3 shows a typical DAIM map (Fig. 3c) and AIM image (Fig. 3d) from the forepaw electrical stimulation group. While the DAIM map was generally well contained to the somatosensory cortex, the AIM image showed significant contamination from nonspecific activation, such as in ventricular regions (arrows), and also in medial and lower regions of the brain.

Table 1 shows a comparison of DAIM values and relative AIM signal enhancement. In the glutamate administration group, DAIM values in the brain hemisphere were significantly higher compared to values in the ventricles ($P < 0.001$, $N = 5$). In contrast, in the AIM MRI, the relative signal enhancement in the brain hemisphere was not significantly different than in ventricles ($P > 0.05$). In the forepaw electrical stimulation group, higher DAIM values were observed in the primary somatosensory cortex for forelimb region (S1FL) compared to ventricles ($P < 0.001$, $N = 5$). On the other hand, AIM enhancement in the

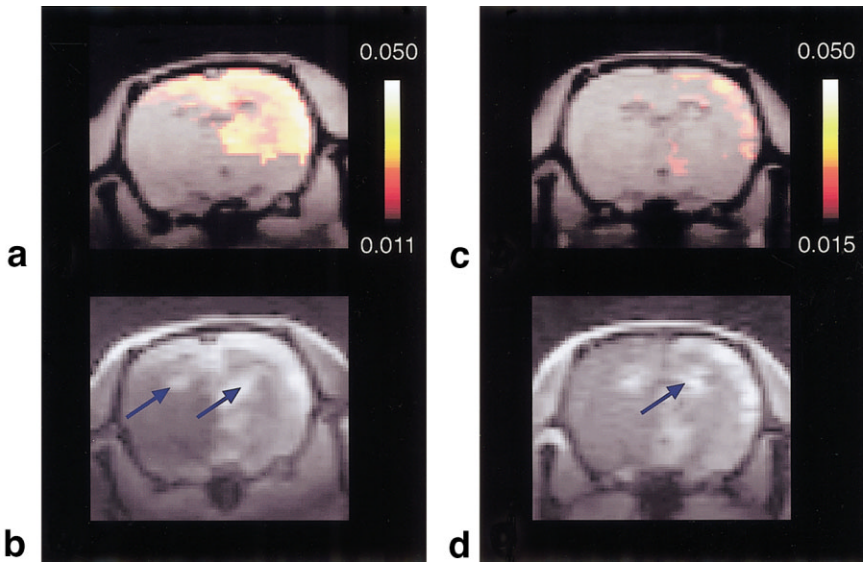

FIG. 3. Comparison between DAIM and AIM MRI. The left column shows (**a**) a typical DAIM functional map and (**b**) AIM images from the glutamate administration group. The right column shows (**c** and **d**) corresponding maps for the forepaw electrical stimulation group. While the (**a** and **c**) DAIM maps only show the regions specifically activated by the stimulation paradigm, the (**b** and **d**) AIM images show contamination from nonspecific activation, such as ventricles (arrows).

Table 1
Comparison of DAIM Values and Relative AIM Signal Enhancement for Different Brain Regions During Glutamate Administration and Electric Forepaw Stimulation

Type of stimulus	Brain region	DAIM value[a]	Relative AIM MRI signal enhancement[b]
Glutamate administration	Right hemisphere (except ventricles)	0.037 ± 0.005	174 ± 35%
	Ventricles	0.012 ± 0.003	155 ± 21%
Electric forepaw stimulation	S1FL	0.028 ± 0.003	131 ± 20%
	Cortex (except S1FL)	0.018 ± 0.005	129 ± 19%

[a]DAIM values were significantly different between right hemisphere and ventricles in glutamate administration group ($P < 0.001$, $N = 5$), and between S1FL and cortex in the electric forepaw stimulation group ($P < 0.001$, $N = 5$).
[b]AIM enhancement in the right hemisphere was not significantly different from enhancement in the ventricles ($P > 0.05$, $N = 5$) in the glutamate administration group. In the electrical forepaw stimulation group, AIM enhancement in SIFL was not significantly different than in other cortical areas ($P > 0.005$, $N = 5$).

somatosensory cortex was identical to enhancement in other cortical regions ($P > 0.05$, $N = 5$).

DISCUSSION

The present work demonstrates that an acquisition paradigm can be used to separate stimulation-specific brain activation from nonspecific signal enhancement during Mn^{2+} delivery to the brain. A functional brain map, referred to as the DAIM map, was produced using the variation of the logarithmic slope of the time-course of signal changes before and during stimulation. Two types of stimulation were used to test the new technique: signal changes were measured in the brain during Mn^{2+} infusion after glutamate administration, and in the somatosensory cortex during electrical stimulation of the forepaw. In both cases, the results were similar to those previously published (3,14). Analyzing time-courses using the DAIM technique helped to eliminate nonspecific effects. These nonspecific effects come from non-activity-dependent signal enhancements due to Mn^{2+} uptake in the ventricles during glutamate administration, and from activity in regions of the cortex not specifically associated with electrical stimulation of the forepaw due to light anesthetic levels. It was shown that the DAIM technique was able to sort out significant differences between specific and nonspecific signal enhancements, although such differences could not be observed with AIM MRI under the conditions used.

The T_1-weighted contrast of AIM MRI is dependent on the anesthetic condition of the animal being examined (15). Signal enhancements in wide areas of the brain were reported without stimulation in AIM MRI using animals that were awake or under light anesthesia (3,15–17). We have also observed a dispersion of signal enhancement in preliminary experiments, which depended on the depth of anesthesia (data not shown). The working hypothesis is that the contrast detected with AIM MRI is produced by the Mn^{2+} influx into neurons through voltage-gated calcium channels caused by depolarization (6–9). This is supported by evidence that calcium channel blockers inhibit Mn^{2+} uptake in isolated cells (6–9), mouse heart (20), and olfactory neurons in the mouse (21). Whether the rate of manganese influx as measured by DAIM in the brain can be quantitatively related to calcium influx or neural activity will require further study. Even under deep anesthesia, brain waves are still observed as a result of neuronal depolarization (18). Therefore, one cannot neglect the possibility that AIM MRI can produce signal enhancements unrelated to specific stimulation. Earlier results using AIM MRI that reported excellent contrast during somatosensory stimulation were obtained under optimized anesthetic conditions for each stimulation (15,16). However, individual differences in anesthetic sensitivity, or even stimulation from the surrounding environment, such as gradient noise or securing of the animal, may produce unintended "activated areas" (15). Therefore, one needs to correct for possible baseline signal increases in AIM MRI while maintaining an appropriate anesthetic depth and physiological stability. Time-course analysis of MRI signals, such as DAIM, has been used widely in perfusion MRI for observing the first pass of gadolinium-based contrast agents (22), in dynamic susceptibility contrast MRI (23), and in brain fMRI using BOLD contrast (24).

The time-course of DAIM indicates several things. First, the influence of Mn^{2+} in blood can be ignored under the conditions used, because there was no significant increase in signal intensity before the BBB was broken, even though manganese infusion had begun. This is consistent with previous studies that did not observe significant signal changes even when blood flow and blood volume were increased with increased arterial CO_2 (3). Therefore, Mn^{2+} is not dependent on hemodynamic changes. This is probably because of the small volume ratio of the vascular bed for brain, and the small Mn^{2+} concentration inside the vessel.

The second set of images, obtained after injection of mannitol, showed a change in signal intensity obtained without specific stimulation. The slope of this nonspecific signal change tracks the increase in Mn^{2+} influx caused by stimulation from the environment, such as noise, light, and/or holding the animal. The slope was different from that obtained in the third set of images, during which changes in signal intensity were observed as a result of specific stimulation (glutamate administration or electrical forepaw stimulation), in addition to the nonspecific stimulation from the environment. The DAIM value and map eliminates the influence of the nonspecific signal changes by retaining the signal changes from the specific stimulation only. Because the maps are generated by taking the log

of the signal changes and then subtracting the resulting slopes, when the DAIM value is positive the signal changes caused by specific stimulation are bigger than the nonspecific changes. Likewise, when the DAIM value is negative, the changes caused by specific stimulus are smaller than the changes caused by nonspecific stimulation. Therefore, the DAIM values and map can discriminate between increases and decreases of baseline activity. This may be useful for mapping inhibitory as well as excitatory effects.

It is well known that glutamate administrated from the carotid artery with a broken BBB induces depolarization of neurons throughout the brain (25). It was also reported that Mn^{2+} causes an increase of signal intensity in the ventricle and choroid plexus during AIM MRI (15), even though there are no neurons in this region. The mechanism by which the ventricle accumulates Mn^{2+} is not known. The ventricle, which has high signal intensity using AIM MRI, did not show high intensity on the DAIM maps (Table 1). This result shows that DAIM maps have the ability to exclude signal increases that occur due to nonspecific effects. On the other hand, it is well known that electrical forepaw stimulation induces the localized depolarization of neurons in the S1FL (26,27). Furthermore, a previous study compared AIM with fMRI techniques and detected similar regions activated by forepaw stimulation (14). In the present work, wherein low levels of anesthesia were used, the increase in signal intensity by electrical forepaw stimulation was also observed in other regions of cortex, in addition to S1FL (Fig. 3). It is hypothesized that the causes of these signal increases are disinhibition, basal neuronal activity, and unintended stimulation from the environment, such as sound, light, and restraint of the animal (3). In a previous work, manganese was given to the animal outside the MRI in a better-controlled environment, which led to less nonspecific stimulation (3). That DAIM MRI increased specificity is demonstrated by the fact that there was no difference on AIM MRI between S1FL and other regions of the cortex under the anesthetic conditions used in this study; however, the DAIM map did detect the stimulation-specific region in the brain.

DAIM MRI has some similarities to the widely used deoxyglucose method of mapping brain function (28,29). With deoxyglucose, the rate of glucose uptake is measured by the metabolic trapping of deoxyglucose and is quantified. Areas with higher rate of glucose uptake are interpreted as areas with higher activity. Manganese is most likely sensitive to calcium influx, rather than to metabolic rates, since it enters cells efficiently on voltage-gated calcium channels. Calcium influx is an essential step in neurotransmission. Once inside cells, manganese is not efficiently exported on short time scales. Mn^{2+} can bind to magnesium- and iron-binding sites as well as to calcium sites, so once it enters cells there is a large number of potential binding sites. It may be possible to make use of the other biological properties of Mn^{2+} to sensitize MRI to other processes in addition to ion influx through voltage-gated calcium channels. Indeed, it has been demonstrated that Mn^{2+} will track along appropriate neuronal pathways, making it possible to use manganese-enhanced MRI (MEMRI) for neuronal track tracing (21). Whether Mn^{2+} is mimicking another biological ion or this is a specific transport process for Mn^{2+} is yet to be determined.

The DAIM paradigm that detects stimulation-specific activation provides a method for functional brain analysis. This method can be used to eliminate nonspecific effects on quantitative T_1-calculated AIM maps, and the need to carefully optimize anesthetic levels during AIM MRI. Because the DAIM paradigm can be performed simultaneously with AIM MRI on the same animal, it complements AIM MRI, which can have high spatial resolution and high SNR. The DAIM method should be useful in many applications for mapping calcium influx using manganese-enhanced MRI. In addition, it is possible to use Mn^{2+} to monitor other types of excitable cells, such as myocytes and pancreatic beta cells, using DAIM, and for pathological conditions such as the excito-toxic effects associated with stroke (30).

CONCLUSIONS

DAIM MRI is a useful technique for separating stimulation-specific signal enhancement from nonspecific signal enhancement in the rat brain using manganese as a functional contrast agent. Using the DAIM paradigm as an experimental methodology, calculated functional maps were obtained as an analytical tool for detecting specific brain activation. It was shown that DAIM maps are more specific for imaging brain activation with glutamate administration and electrical forepaw stimulation compared with AIM MRI. The DAIM method will be useful for baseline correction of AIM MRI in animals under light anesthesia, and even in alert animals.

ACKNOWLEDGMENTS

The authors thank Dr. F. Mitsumori (National Institute for Environmental Studies, Japan), Dr. M. Kumagai (University of Tsukuba School of Medicine, Japan), and Dr. K. Kawakita for stimulating discussions; Ms. A. Nakagoshi and Mrs. T. Aoki for assisting in the animal procedures; and Mr. Y. Watanabe, Mr. Y. Someya, and Mr. Y. Mori for their assistance in this study.

REFERENCES

1. Ogawa S, Lee TM, Kay AR, Tank DW. Brain magnetic resonance imaging with contrast dependent on blood oxygenation. Proc Natl Acad Sci USA 1990;87:9868–9872.
2. Detre JA, Leigh JS, Williams DS, Koretsky AP. Perfusion imaging. Magn Reson Med 1992;23:37–45.
3. Lin YJ, Koretsky AP. Manganese ion enhances T_1-weighted MRI during brain activation: an approach to direct imaging of brain function. Magn Reson Med 1997;38:378–388.
4. Hunter DR, Komai H, Haworth RA, Jackson MD, Berkoff HA. Comparison of Ca^{2+}, Sr^{2+}, and Mn^{2+} fluxes in mitochondria of the perfused rat heart. Circ Res 1980;47:721–727.
5. Shibuya I, Douglas WW. Indications from Mn-quenching of Fura-2 fluorescence in melanotrophs that dopamine and baclofen close Ca channels that are spontaneously open but not those opened by high $[K^+]O$; and that Cd preferentially blocks the latter. Cell Calcium 1993; 14:33–44.
6. Kita H, Narita K, Van der Kloot W. Tetanic stimulation increases the frequency of miniature end-plate potentials at the frog neuromuscular junction in Mn^{2+}-, CO^{2+}-, and Ni^{2+}-saline solutions. Brain Res 1981; 205:111–121.

7. Drapeau P, Nachshen DA. Manganese fluxes and manganese-dependent neurotransmitter release in presynaptic nerve endings isolated from rat brain. J Physiol (Lond) 1984;348:493–510.
8. Burnett KR, Goldstein EJ, Wolf GL, Sen S, Mamourian AC. The oral administration of $MnCl_2$: a potential alternative to IV injection for tissue contrast enhancement in magnetic resonance imaging. Magn Reson Imaging 1984;2:307–314.
9. Narita K, Kawasaki F, Kita H. Mn and Mg influxes through Ca channels of motor nerve terminals are prevented by verapamil in frogs. Brain Res 1990;510:289–295.
10. Mendonca DM, Gaggelli E, Lauterbur PC. Paramagnetic contrast agents in nuclear magnetic resonance medical imaging. Semin Nucl Med 1983;13:364–376.
11. Geraldes CF, Sherry AD, Brown Rd, Koenig SH. Magnetic field dependence of solvent proton relaxation rates induced by Gd^{3+} and Mn^{2+} complexes of various polyaza macrocyclic ligands: implications for NMR imaging. Magn Reson Med 1986;3:242–250.
12. Cory DA, Schwartzentruber DJ, Mock BH. Ingested manganese chloride as a contrast agent for magnetic resonance imaging. Magn Reson Imaging 1987;5:65–70.
13. Fornasiero D, Bellen JC, Baker RJ, Chatterton BE. Paramagnetic complexes of manganese(II), iron(III), and gadolinium(III) as contrast agents for magnetic resonance imaging. The influence of stability constants on the biodistribution of radioactive aminopolycarboxylate complexes. Invest Radiol 1987;22:322–327.
14. Duong TQ, Silva AC, Lee SP, Kim SG. Functional MRI of calcium-dependent synaptic activity: cross correlation with CBF and BOLD measurements. Magn Reson Med 2000;43:383–392.
15. Lin YJ. An approach to direct imaging of brain activation with MRI by activity-induced manganese dependent, "AIM", contrast. Pittsburgh: Carnegie Mellon University; 1997. 261 p.
16. Aoki I. Evaluation of brain activation with acupuncture stimulation using activity-induced manganese dependent contrast MRI in the rat. Hiyoshi-cho, Kyoto, Japan: Meiji University of Oriental Medicine; 1999.
17. Aoki I, Tanaka C, Takegami T, Ebisu T, Umeda M, Fukunaga M, Someya Y, Watanabe Y. Experimental functional MRI using dynamic activity-induced manganese dependent contrast (DAIM). In: Proceedings of the 7th Annual Meeting of ISMRM, Philadelphia, 1999. p 359.
18. Schmidt KF. Effect of halothane anesthesia on regional acetylcholine levels in the rat brain. Anesthesiology 1966;27:788–792.
19. Kumagai M, Toyooka H, Mitsumori H. Brain functional mapping using manganese ion. In: Proceedings of the Japan Society for Magnetic Resonance in Medicine, Tokyo, 1999. p 149.
20. Hu TC-C, Pautler GP, MacGowan GA, Koretsky AP. Manganese enhanced MRI of the mouse heart during changes in inotropy. Magn Reson Med 2001;46:884–890.
21. Pautler RG, Silva AC, Koretsky AP. In vivo neuronal tract tracing using manganese-enhanced magnetic resonance imaging. Magn Reson Med 1998;40:740–748.
22. Villringer A, Rosen BR, Belliveau JW, Ackerman JL, Lauffer RB, Buxton RB, Chao YS, Wedeen VJ, Brady TJ. Dynamic imaging with lanthanide chelates in normal brain: contrast due to magnetic susceptibility effects. Magn Reson Med 1988;6:164–174.
23. Levin JM, Kaufman MJ, Ross MH, Mendelson JH, Maas LC, Cohen BM, Renshaw PF. Sequential dynamic susceptibility contrast MR experiments in human brain: residual contrast. Magn Reson Med 1995;34:655–663.
24. Bandettini PA, Jesmanowicz A, Wong EC, Hyde JS. Processing strategies for time-course data sets in functional MRI of the human brain. Magn Reson Med 1993;30:161–173.
25. Dingledine R, McBrain CJ. Excitatory amino acid transmitters. In: Siegal GJ, Agranoff BW, Albers RW, Molinoff PB, editors. Basic neurochemistry: molecular, cellular and medical aspects. New York: Raven Press, Ltd.; 1994. p 367–387.
26. Hyder F, Behar KL, Martin MA, Blamire AM, Shulman RG. Dynamic magnetic resonance imaging of the rat brain during forepaw stimulation. J Cereb Blood Flow Metab 1994;14:649–655.
27. Gyngell ML, Bock C, Schmitz B, Hoehn-Berlage M, Hossmann KA. Variation of functional MRI signal in response to frequency of somatosensory stimulation in alpha-chloralose anesthetized rats. Magn Reson Med 1996;36:13–15.
28. Sokoloff L, Reivich M, Kennedy C, Des Rosiers MH, Patlak CS, Pettigrew KD, Sakurada O, Shinohara M. The [^{14}C] deoxyglucose method for the measurement of local cerebral glucose utilization: theory, procedure, and normal values in the conscious and anesthetized albino rat. J Neurochem 1977;28:897–916.
29. Phelps ME, Huang SC, Hoffman EJ, Selin C, Sokoloff L, Kuhl DE. Tomographic measurement of local cerebral glucose metabolic rate in humans with (F-18)2-fluoro-2-deoxy-D-glucose: validation of method. Ann Neurol 1979;6:371–388.
30. Aoki I, Tanaka C, Ebisu T, Katsuta K, Fujikawa A, Umeda M, Fukunaga M, Watanabe Y, Someya Y, Fukuda K, Takegami T, Naruse S. Mismatch between the manganese ion influx and decreased apparent diffusion coefficient of water in the focal ischemia. In: Proceedings of the 8th Annual Meeting of ISMRM, Denver, 2000. p 2012.